Title

Solid-State NMR Investigations of Carbon Dioxide Gas in Metal–Organic Frameworks: Insights into Molecular Motion and Adsorptive Behavior

Journal

Chemical Reviews, 118(20)

ISSN

0009-2665

Authors

Witherspoon, Velencia J
Xu, Jun
Reimer, Jeffrey A

Publication Date

2018-10-24

DOI

10.1021/acs.chemrev.7b00695

Peer reviewed

CHEMICAL REVIEWS

Review

Cite This: *Chem. Rev.* 2018, 118, 10033−10048

pubs.acs.org/CR

Solid-State NMR Investigations of Carbon Dioxide Gas in Metal−Organic Frameworks: Insights into Molecular Motion and Adsorptive Behavior

Velencia J. Witherspoon, Jun Xu, and Jeffrey A. Reimer*

Department of Chemical and Biomolecular Engineering, University of California, Berkeley, Berkeley, California 94720, United States

Supporting Information

ABSTRACT: Solid-state nuclear magnetic resonance (SSNMR) methods have been routinely used for the characterization of both the structure and the dynamics of metal organic frameworks (MOFs), a collection of porous media investigated for potential applications in carbon capture technologies, selective separation of small molecules, and catalysis.[1] The use and development of SSNMR techniques that enable the nondestructive characterization of the adsorbed behavior have become essential steps in bettering our understanding of MOFs and are often complementary to traditional methods of structural characterization. This Review aims to give a brief introduction to the relevant concepts of SSNMR and the methods employed when investigating the phenomenon of adsorbed carbon dioxide gas in MOFs. We summarize the published SSNMR literature on CO_2 in MOFs, as well as highlight the best experimental practices when working with these complex systems.

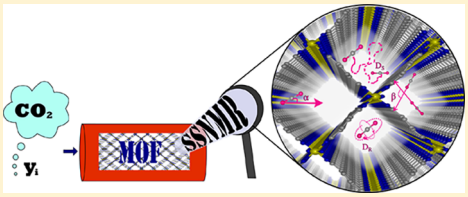

CONTENTS

1. INTRODUCTION

1.1. Understanding Gas Dynamics in MOFs

One of the most promising classes of solid adsorbate materials for CO_2 capture technologies are metal−organic frameworks, MOFs.[2] These materials consist of a diverse set of secondary building units (SBUs) typically comprised of metal oxide clusters and organic monomers that self-assemble into a network of coordination bonds, yielding a porous framework. Researchers can "tune" both the metals and the SBUs to facilitate control of pore size, pendant chemistry, and geometry[3,4] so as to directly influence material properties and performance in a particular application. For example, many researchers have begun to design and modify SBUs to enable favorable host−guest interactions in MOFs for carbon capture and storage technologies.[5] Experimental techniques that allow for methodical characterization of host−guest interactions, however, are needed to develop structure−property relationships for MOF−CO_2 systems. Methods such as adsorption isotherms, differential scanning calorimetry (DSC), thermogravimetric analysis (TGA), and X-ray diffraction (XRD) are

Received: November 17, 2017
Published: October 5, 2018

DOI: 10.1021/acs.chemrev.7b00695
Chem. Rev. 2018, 118, 10033−10048

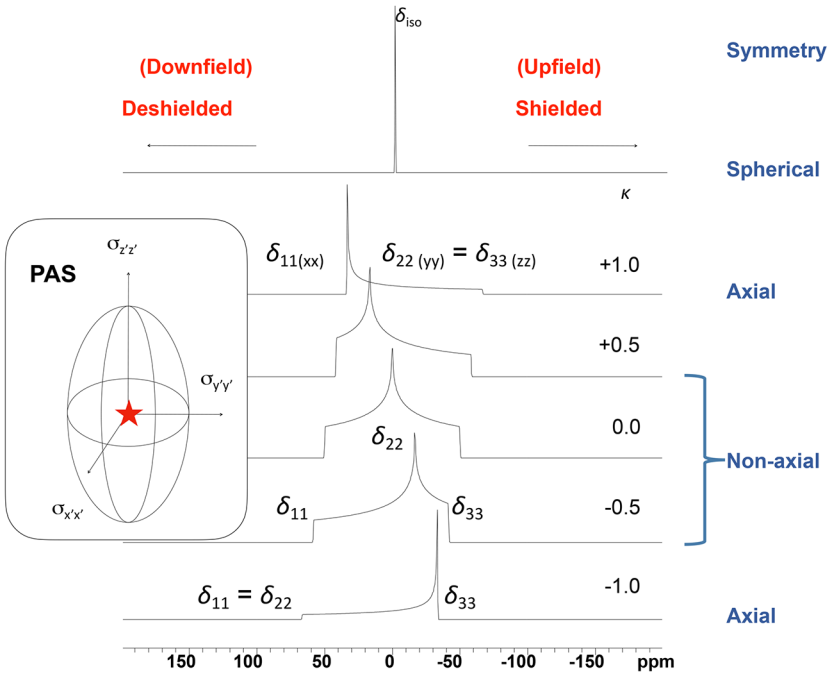

Figure 1. NMR "powder patterns" associated with the chemical shift anisotropy using the Herzfeld–Berger convention. In this example, Ω = 100 ppm, δ_{iso} = 0 ppm. The NMR active nucleus is indicated by a star, and the principal axis system (PAS) is oriented relative to the local environment (e.g., chemical bonds) via a set of Euler angles (not shown). The powder patterns are characterized by the "singularity" and the "shoulders"; for example, in the bottom powder pattern the singularity is characterized by δ_{33} and the shoulder by $\delta_{11} = \delta_{22}$.

often used to probe the thermodynamics describing these interactions,[6] but these methods have limitations when seeking to inclusively understand thermodynamics, kinetics, and transport of CO_2 in MOFs to improve materials design.[7]

Nuclear magnetic resonance (NMR) has proven capable of observing fluctuations of local bonding environments in MOF–adsorbate systems, often yielding information about local interactions and the motion of the adsorbed molecules.[8] Solid-state nuclear magnetic resonance (SSNMR) has been successful in characterizing the structure of MOF frameworks[9] and has been previously employed toward the elucidation of the structure of catalysts and catalytic processes.[10] This Review will focus on introducing the fundamentals of SSNMR for describing adsorbed CO_2 and how this understanding discerns the intricacies of physisorption processes in various classes of MOFs. We will discuss how SSNMR has been essential for the determination of adsorption site(s) and mechanism(s), as well as the molecular dynamics associated with the bound sorbate. This information improves the design of MOFs function as a material for carbon capture technologies.

1.2. Introduction to Solid-State NMR of Adsorbed CO_2

SSNMR may capture local dynamics through interpretation of NMR observables such as chemical shift anisotropy (CSA),[11,12] dipolar and quadrupolar interactions,[13] as well as motion-dependent NMR observables such as the spin–spin relaxation time (T_2), and spin–lattice relaxation time (T_1),[14] and self-diffusion coefficients.[15] Although difficult to interpret, these observables can provide a clear description of the CO_2–framework interactions. SSNMR is best known as a structural characterization tool, and this Review will focus on the SSNMR characterization of host–guest interactions and its contribution toward understanding the CO_2 adsorbed in MOFs. To begin, we reintroduce some basic concepts that enable the use of SSNMR, omitting for the sake of brevity information on the origins of NMR spectroscopy, which can be found elsewhere.[13,16] Most important, however, is the chemical shift interaction as it affords the association of observed spectral resonances with the local bonding environment of the nuclei being observed.

In diamagnetic solids, the chemical shielding interaction is usually a nonisotropic property deriving from the electronic shielding or deshielding of the nucleus in the applied NMR magnetic field. The local magnetic field at a given nucleus is modified by the electronic structure of the molecule or solid and possesses a directionality and a magnitude best described by an absolute shielding tensor, $\hat{\sigma}$, that determines the total contribution to the overall magnetic field felt by the observed nucleus.

$$B_i = (1 - \hat{\sigma})\cdot B_0 \quad (1)$$

The shielding tensor $\hat{\sigma}$ may be thought of as the difference between the frequency of the bare nucleus and the nucleus in a chemical environment (chemical bonds, molecules in solution, solid crystals, etc.). The second-rank chemical shielding tensor $\hat{\sigma}$ is fixed in the molecular frame via the principal axis system (PAS); the isotropic chemical shielding is calculated from the on-diagonal values of the diagonalized shielding tensor (σ_{11}, σ_{22}, σ_{33}) as shown in Figure 1. The largest component of the shielding tensor, σ_{11}, is defined by convention to be along the z-axis of PAS, while σ_{22} and σ_{33} are along the x- and y-axes, respectively.[17] A completely unshielded nucleus has a resonance frequency associated with the Larmor frequency, $\omega_0 = B_0\gamma$; the shielding tensor contributes to a shift in the observed resonance frequency $\omega_i = B_i\gamma$,[18] where B_i is given by eq 1 and γ is the tabulated nuclear magnetogyric ratio, a property of the atomic nucleus.

DOI: 10.1021/acs.chemrev.7b00695
Chem. Rev. 2018, 118, 10033–10048

The NMR community typically uses chemical shifts (symbol δ) and not shielding as the way to express and analyze experimental data. These shifts are calculated as the difference between the observed NMR frequency, ω_i, and a reference frequency, ω_{ref}, taken from an IUPAC standard compound.[19] Chemical shifts are dimensionless and reported in ppm (parts per million) of the overall magnetic field, $\delta_i = 10^6\left\{\frac{\omega_{ref}-\omega_i}{\omega_{ref}}\right\}$. The shielding tensor $\hat{\sigma}$ in eq 1 is then replaced with the chemical shift tensor $\hat{\delta}$.

It is tempting to eschew the linear algebra associated with tensor quantities such as chemical shifts. In the description of surface-adsorbed molecules, and CO_2 in particular, this is ill-advised as the rotational dynamics of CO_2 on surfaces underpins the energetics of adsorption, desorption, and transport. Fortunately, we can succinctly deal with this by recalling that the second-rank shift tensor $\hat{\sigma}$ is described by a 3 × 3 matrix. This matrix is further decomposed into the sum of three submatrixes, with each submatrix being identified by how it transforms under rotation in real space (hence the connection to molecular dynamics).

To see how these rotations are expressed, consider an arbitrary chemical shift tensor $\hat{\delta}$:

$$\hat{\delta} = \begin{pmatrix} \delta_{11} & \delta_{12} & \delta_{13} \\ \delta_{21} & \delta_{22} & \delta_{23} \\ \delta_{31} & \delta_{32} & \delta_{33} \end{pmatrix}$$

The trace $Tr\hat{\delta} = \sum\delta_{ii} = \delta_{11} + \delta_{22} + \delta_{33} = \delta_0$ is easily calculated and may be subtracted form the original $\hat{\delta}$ to yield:

$$\hat{\delta} = \hat{\delta}_0 + \hat{\delta}_{remainder}$$

The elements of $\hat{\delta}_o$ are such that its trace is that of $\hat{\delta}$, but its other components are zero.

Consider the remainder matrix. The off-diagonal elements of this tensor, $\hat{\delta}_{ij}$ and $\hat{\delta}_{ji}$, need not have the same value. One may write, however, an antisymmetric and a symmetric combination of these:

$$\delta^a_{ij} = \frac{1}{2}(\delta_{ij} - \delta_{ji})$$

and

$$\delta^s_{ji} = \frac{1}{2}(\delta_{ij} + \delta_{ji})$$

When added together, these give the appropriate off-diagonal element of $\hat{\delta}$. One may assign a value of zero to each diagonal element $\hat{\delta}^a$, and a value $\delta_{ii} - \delta_0/3$ to the diagonal elements of $\hat{\delta}^s$. As a result, one sees that the original tensor of rank two can be parsed into three, each of which behaves under rotation in a certain way:

$$\hat{\delta} = \hat{\delta}_0 + \hat{\delta}^a + \hat{\delta}^s$$

As we have seen, $\hat{\delta}$ transforms under rotations like a scalar, which is to say that it is unaffected by rotations. The second term, $\frac{1}{2}(\delta_{ij} - \delta_{ji})$, has the form of a cross product between two vectors, so it transforms under rotation like a vector. The totally symmetric, traceless tensor, $\frac{1}{2}(\delta_{ij} + \delta_{ji})$, has six independent parameters, three off-diagonal elements, and three diagonal elements. However, because the trace has been subtracted off, there are only five independent elements.

The original tensor $\hat{\delta}$ had nine independent Cartesian elements. In the representation as a sum of $\hat{\delta}_0$, $\hat{\delta}^a$, and $\hat{\delta}^s$ tensors, it still has nine independent elements, but they are parsed into parts that have specific symmetry properties under rotation. In particular, each looks like an object having angular momentum equal to 0 (scalar), 1 (vector), and 2 (tensor), respectively. It is beyond the scope of this Review to dwell further on the quantum mechanics of angular momentum, but a theorem in quantum mechanics shows that the vector (antisymmetric) components of the chemical shift tensor are not observable in standard NMR experiments. The scalar is unaffected by rotations, and the symmetric components transform under rotations such as spherical harmonics of rank 2 that contain the second-order Legendre polynomial $P_2 \cos\theta$.

These transformation properties become important when the NMR-observed molecules undergo rotation as part of their adsorption dynamics, and/or when the sample is mechanically rotated by the experimenter. The latter case is known as "magic angle spinning" (MAS) wherein the sample is rapidly rotated at the angle 54.7° relative to the applied magnetic field. This angle is the root of $P_2 \cos\theta(\propto 1-3\cos^2\theta) = 0$ and results in averaging to zero the symmetric component of the chemical shift tensor. All that remains under MAS is the scalar portion of the chemical shift, that is, $\delta_{iso} = \frac{1}{3}(\delta_{11} + \delta_{22} + \delta_{33})$,[17] the same shift as one would observe in liquid-state NMR where fast Brownian motion yields only the isotropic elements of the shielding tensor.[20] In the case of CO_2, this yields a single observed or isotropic chemical shift of about 128 ppm (relative to the shift standard TMS: tetramethylsilane) for gas or liquid NMR spectrum. In the case of an adsorbed molecule, however, random motions may not be significant enough to completely average away nonisotropic components of the chemical shielding tensor. In these cases, the observed spectrum maps the orientation-dependent angular motion (e.g., rotation about a C_3 axis) onto the second-rank shielding tensor, yielding "powder patterns" that are modified from the static case.[21]

Historically, there are multiple conventions employed to describe the anisotropy of the chemical shift tensors in reference to the molecular frame. The most common convention used for CO_2 in the MOF literature is the "Herzfeld–Berger" convention.[19] In the Herzfeld–Berger convention, the three components used to describe the anisotropy of chemical shift tensor are the span $\Omega = \delta_{11}-\delta_{33}$; the isotropic chemical shift value δ_{iso}; and the skew $\kappa = \frac{3(\delta_{22}-\delta_{iso})}{\Omega}$, which orders the respective values of the chemical shift tensor components to $\delta_{11} \geq \delta_{22} \geq \delta_{33}$. In this Review, all data collected use this "Herzfeld–Berger" convention, although a few papers are discussed exclusively in other conventions. The notation in Figure 1 for the characteristic terms of the chemical shift interaction follows this IUPAC convention.

The linear nature of the carbon dioxide molecule[22] facilitates the interpretation of NMR powder patterns in terms of the dynamic reorientation of the molecule. The z-axis of the PAS is assigned to be parallel to the carbon–oxygen bond, and when the molecular axis of rotation is pinned along one of the oxygen atoms, the deduction of reorientation at adsorption sites within the framework[23] is straightforward (Figure 2). This simplification, when paired with NMR simulation software,[12,24] can quantitatively reproduce experimental spectra. When CO_2 molecules are not chemisorbed to the surface, physisorption

DOI: 10.1021/acs.chemrev.7b00695
Chem. Rev. 2018, 118, 10033–10048

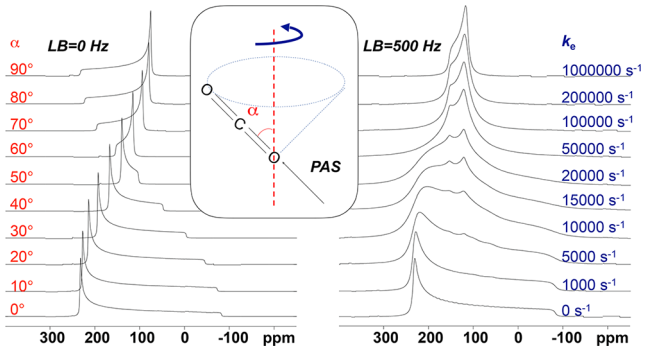

Figure 2. Inset shows the relevant geometries for the linear CO_2 molecule bound to a surface through a single oxygen atom. The dashed red line depicts the rotation axis. The *z*-axis of the chemical shift PAS is taken to be along the O═C═O bond. (Left) In this rotational model, the calculated chemical shift powder patterns emanating from ^{13}C nuclei in CO_2 molecules are shown. Note how the breadth of these patterns changes with the angle (center inset) the bound molecule makes relative to the surface and the PAS. Indeed, the pattern appears to "flip" the singularity and shoulder of the powder pattern as the angle passes through about 54°, the root of the equation $1 - 3\cos^2\theta = 0$. (Right) Given an α of 60°, the calculated chemical shift powder patterns for adsorbed CO_2 as a function of the rate at which rotation about α occurs. These calculated spectra demonstrate well how the observed NMR spectra from adsorbed CO_2 can be readily interpreted in terms of adsorbate dynamics.

results in the molecule attaching and detaching at a frequency dictated by the energetics of framework−guest interactions.[8] In these circumstances, adsorbate−MOF powder patterns are a sum of resonances emanating from each molecule as differentiated by the specific combination of molecular motions and relative orientations.

1.3. Simulation Software for Analysis of Spectra

Comparison of experimental and simulated powder patterns as a function of temperature is often used to assess the energetics of molecular motion, including the preferred adsorbed molecular orientation and its influence on adsorbate mobility in the pore.[25,26] Molecular motions such as rotation, wobbling, pendulum-like swinging, or hopping between adsorption sites affect the observed spectra, where the type of motion and the rate of the motion can cause either narrowing or broadening of the recorded powder patterns.[27] Although there are many ways to simulate orientation- and motion-dependent behavior of linear CO_2, we choose to highlight two of the most commonly used software packages for these applications: a MATLAB-based package called EXPRESS[12] and the Tcl/C-based package SIMPSON.[24] SIMPSON functions as a "computerized spectrometer" that allows for the numerical simulation of SSNMR observables wherein the user inputs the desired experiment, the number of spins, and some of the details for numerically sampling the differing orientations of molecular, PAS, and motional axes. SIMPSON numerically evaluates the Louiville von-Neumann equation of motion for the density matrix of a large ensemble of spins. This differential equation effectively describes the time equation of motion for nuclear spins subject to time-dependent nuclear spin interactions, for example, the chemical shift tensor in the presence of molecular motion and the presence of RF pulses. The advantage of SIMPSON is that it provides a series of files that list of orientations over which the equations of motion may be averaged to represent the observed chemical shift powder pattern. EXPRESS allows users to use a GUI to implement simulations of NMR spectra; yet because it is MATLAB-based it also affords user-input and modification directly using this popular software. The advantage of EXPRESS is that it enables easy inclusion of the site-to-site "jump" dynamics that often describe adsorbed gases; it also applies inhomogeneous broadening due to fast or slow exchange between these preferentially occupied sites, thereby allowing for direct comparison to experimental spectra. EXPRESS allows the user to input the posited orientations of the nuclear spin system and to modify the respective population between these orientations. Figure 2 shows how rapid, uniaxial rotation of the CO_2 about a single oxygen atom bonded to the surface yields simulated powder patterns on the basis of the angle of the uniaxial rotation. The right-hand side of Figure 2 details how the rate of uniaxial rotation affects the powder pattern for a given angle of rotation with respect to the surface.

Adsorbate motion is a thermodynamically driven process; thus the energy barrier for types of motion may be investigated using variable-temperature experiments accompanied by an Eyring or Arrhenius analysis.[26,28] Although adsorbed CO_2 most commonly results in a powder pattern spectrum associated with a single adsorption site, it is possible that adsorption may produce distinct chemical shifts between differing adsorption sites, as shown in Figure 3. In this case, the exchange between these environments due to adsorbate motion may also be investigated as a function of temperature. The degree of overlap between these NMR peaks is

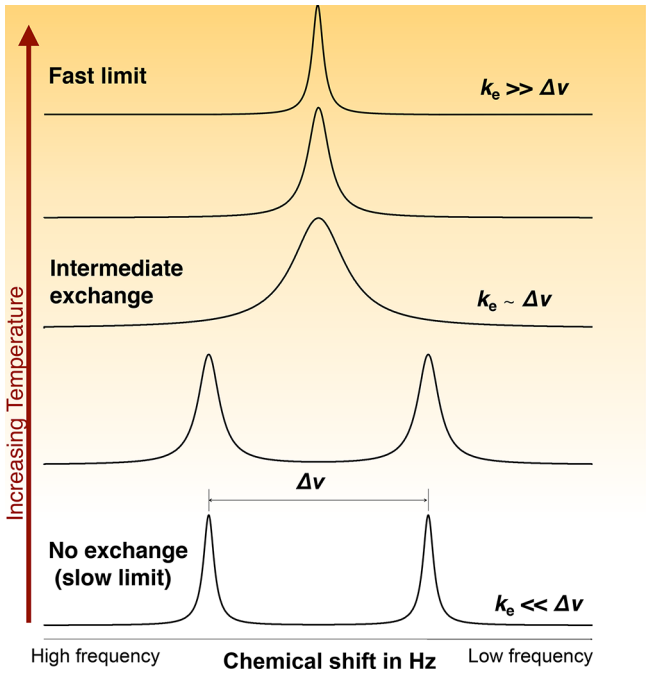

Figure 3. Spectra representing observed NMR lineshapes for molecules undergoing exchange between two sites of differing isotropic chemical shift. At the bottom are the spectra associated with the two sites in the absence of exchange; two distinct chemical environments are observed. As the rate of the exchange between sites increases, the lines broaden, merge, then narrow again as it approaches the fast exchange limit wherein the rate of exchange is much faster than the frequency separation of the two peaks. In the fast exchange limit, the motion is said to be "faster than the NMR time scale".

DOI: 10.1021/acs.chemrev.7b00695
Chem. Rev. 2018, 118, 10033−10048

determined by the frequency of the exchange relative to the observed NMR frequency difference between the corresponding environments. When the temperature is high enough, the exchange rate exceeds the difference in frequencies between the chemical shifts associated with the two environments and a single NMR peak is observed; similarly, at low temperature, the exchange is limited and the peaks are easily distinguished from one another. It is difficult to observe exchange phenomena with proton spectra of adsorbates due to the combination of a smaller chemical shift range (hence difference in frequencies) and the effects of other nuclear spin interactions, such as the homonuclear dipole−dipole interaction. Contrarily, the ^{13}C chemical shift range is ∼200 ppm, making it possible to resolve the peaks and quantify exchange rates.

NMR spectroscopy is one of the least sensitive spectroscopic methods available. This is particularly true when observing a nuclear such as ^{13}C by direct, pulsed excitation at the carbon-13 Larmor frequency. Enhancement of NMR signals is possible with a number of schemes; yet one dominates the literature of $^{13}CO_2$: cross-polarization (CP). The detailed spin physics for this process is beyond the scope of this Review. Briefly, the population differences of the nuclear spin states in the applied laboratory field determine the amplitude of the NMR signal. Nuclei that possess larger magnetic moments, such as protons and fluorine, have larger population differences than those (e.g., ^{13}C) with smaller moments. Judicious application of NMR pulses at both the proton and the carbon Larmor frequencies can transfer population differences from the larger moment nucleus to the smaller, thereby enhancing considerably the small-moment NMR signals.[29] This effect is predicated on the presence of nuclear dipole−dipole interactions (see below), which in turn are present only in systems undergoing limited molecular motion. The NMR pulses to accomplish this transfer must meet a specified experimental condition known as Hartman−Hahn matching, causing both the large-moment and the small-moment nuclei to nutate at the same rates, thereby enabling an energy-matching condition that affords population transfer. The efficiency of the CP scheme is very sensitive to the spatial proximity of the two different nuclei.[30] Thus, CP may be applied to enhance the signal of $^{13}CO_2$ when it is in proximity to protons, for example, when $^{13}CO_2$ is bound to a proton-containing substrate.

1.4. Observations of Molecular Motion through Relaxometry and Diffusometry

NMR spectra result from the time Fourier transformation of NMR signals that emanate from the NMR probe circuit. As shown above, these spectra may be interpreted in terms of molecular structure (e.g., the chemical shift tensor $\hat{\delta}$) and the changes it undergoes with motion. Long before Fourier transform NMR, however, NMR spectroscopists focused on the rate constants associated with the NMR signals after perturbation by RF pulses. The rate constant R_1 is the rate at which NMR spin populations return to equilibrium after RF pulses. R_1 is familiar to many by its inverse, T_1, the spin−lattice relaxation time. When the differences in nuclear spin populations over an ensemble of spins are presented as a vector, the equilibrium vector is presented along the z-axis of a Cartesian coordinate system. R_1 is then seen as the rate at which this vector returns to its original z-axis projection after perturbation by RF pulses. The student of routine analytical NMR spectroscopy for use in synthetic chemistry looks to $\frac{1}{R_1} = T_1$ as a metric for the time delay between signal averages. Measurement of R_1, however, may also be used to interrogate the motion of adsorbed molecules.[10,31−33]

A complete analytical description of NMR relaxation times is beyond the scope of this Review and indeed occupies many textbooks.[34] Suffice to say that changing the populations of nuclear spin energy levels necessitates the exchange of energy with the lattice, a euphemism for the bath of fluctuating magnetic fields associated with the motion of atoms comprising the sample. Two concepts associated with fluctuating magnetic fields are essential for recognizing the connection between adsorbate dynamics and relaxation rates. The first is the correlation time τ_c; this may be thought of as the finite time over which the ensemble-averaged correlation of motion persists. Colloquially, this is the time it takes for a moving nuclear spin to forget the location from whence it came. The simplest case is a random walk in which the correlation function is $\tau \propto \exp\frac{-t}{\tau_c}$. The second concept is the spectral density function $J(\omega)$. This is given to be the Fourier transform of the correlation function, but is most easily thought of as the probability that motion gives rise to fluctuating fields at frequency ω. For the simple exponentially decaying correlation function, its Fourier transform yields a Lorentzian $J(\omega) \propto \frac{\tau_c}{1+\omega^2\tau_c^2}$.

The randomly fluctuating magnetic field present due to molecular motion has been formally related to the relaxation R_1. Within this simple model, one finds the dependence of the relaxation rates on τ_c:

$$R_1 = \frac{1}{T_1} = \overline{B}\left(\frac{\tau_c}{1+\omega^2\tau_c^2}\right) \tag{2}$$

Bloembergen, Purcell, and Pound first reported equations similar to these,[20] and hence this approach has the moniker BPP theory of spin relaxation. The random process is often treated as thermally activated where $\tau_c(T) = \tau_c^o \exp\frac{E_a}{RT}$, where E_a is an activation energy for the random modulation process and τ_c^o is the time constant associated with the magnitude of some frequency that describes the maximum rate of random field modulation. The activation energy of the motion may be determined from the slope of this plot, and the value of the maximum in R_1 is determined by the magnitude of the square of the field and τ_c^o. In this way, NMR relaxation is connected to the energetics of adsorbate motions.

What is the ultimate origin of the magnetic fields that fluctuate to provide relaxation? This is an entire field of study, but for adsorbates such as CO_2 the fluctuating magnetic fields emanate from neighboring nuclear spins. Semiclassically, each NMR-active isotope is a small magnetic moment that produces a field; neighboring fields experience dipole−dipole interactions (think of two bar magnets) that depend very strongly on the distance between the spins and their orientation of their internuclear vector with respect to the laboratory magnetic field. These dipolar couplings are referred to as "homonuclear" or "heteronuclear" depending on whether the spins are the same or different, respectively. The standard expression of the spin−lattice relaxation rate as a result of homonuclear dipolar coupling is $R_1 = \frac{1}{T_1} \propto J(\omega_0) + 4J(2\omega_0)$,[34,35] where J is the

DOI: 10.1021/acs.chemrev.7b00695
Chem. Rev. 2018, 118, 10033−10048

spectral density function defined above and ω_o is the NMR Larmor frequency of the nuclei.

The relationship established by Bloembergen, Purcell, and Pound reveals there is an orientational dependence as well as translational dependence of dipole−dipole interaction. In this context, the sampling of local fields around the Larmor frequencies that serves as the driving for the lost of magnetization to the lattice is dominated by the rotational configurational freedom, or the rotation-dependent sampling by the molecule of the local fields.[20] This reorientation couples the nuclear magnetic moment of the nucleus with the rotational angular momentum of the molecule, allowing R_1 to serve as a proxy for rotational motion/diffusion. Confined molecules are expected to have shorter spin−lattice relaxation times with magnitudes and temporal trends correlated with the strength of host−guest interactions.[36] At very low loadings, however, it is possible to observe long relaxation times where reorientation of the molecules has become infrequent.[37] When R_1 is measured as a function of temperature with constant loading, one may determine the activation energy representative of the reorientation process of the observed nuclei. The magnitude of this activation energy reflects molecular motion, that is, the barrier for rotational diffusion, spatial restriction(s) due to the pore geometry, and interactions within the framework or between molecules. R_1 as a function of molecular loading or the adsorbed gaseous density trends as a hyperbola with a maximum, or T_1 trends as a hyperbola with a minimum. If an R_1 maximum is observed in a pure gas system, the maximum point is associated with the collision rate between molecules.[38] In the low density regime of pure gases, the slope of R_1 versus ρ is associated with the rate of binary collisions. In the case of adsorbed gases, there is an intermediate-to-high density regime, where the strength of the interaction with the surface is associated with the slope of the relaxation rate versus gaseous density.[39]

The relaxation mechanism associated with adsorbed CO_2 is more commonly described in the context of adsorbed liquids. Here, reorientation mediated by translational displacements occurs when interactions with the surface of the pore result in hindered or incomplete reorientations about a preferential axis such as the PAS of the molecule or the surface. Strongly adsorbed molecules may only change their orientation according to the topological locations of the adsorption sites within surface pores. These events of reorientation may occur slower than rates of bulk rotational diffusion and translational motion inside the pore; consequentially there are often extended reorientation correlation times that may dominate the relaxation mechanism at lower frequencies. This type of motion results in displacements of molecules along the surface for "strongly adsorbed" systems; this is referred to as surface diffusion. "Weakly adsorbing" systems experience relaxation with contributions from small populations of surface diffusion and large populations of bulk diffusing molecules.[28] For adsorbed CO_2 molecules, there are several interpretations that attribute the meaning of a relaxation maximum to a physical process characterized by a correlation time that matches the Larmor frequency; this may be synonymous with the free gas interpretation for the frequency of collision; associated with the inverse rate of exchange between bound sites directly correlated to the surface diffusion; or representative of the frequency wherein one molecule may encounter another at an adjacent site. All of these events may contribute to the observed relaxation mechanism. For adsorbed liquid species, the difference in relaxivity has been associated with the energy of desorption.[37] Unfortunately, NMR relaxation of adsorbed gases is greatly unexplored, and more systematic studies exploring the behavior of adsorbed gaseous species in well-organized porous media are needed for direct interpretations. This is a great opportunity to utilize NMR for understanding adsorption phenomenon in, for example, MOFs.[36,40]

While spectroscopy and relaxometry quantitate local structure and motion of adsorbed CO_2, the optimal design of macroscopic unit operations requires understanding of bulk transport of gases within porous media. Transport of this type is often characterized with bulk measurements such as breakthrough curves or adsorption isotherms. The connection between bulk transport and microscopic (or "atomistic") motion remains elusive to the experimentalist, but well-explored by simulation and theory. Thus, the direct measurement of the self-diffusivity of, for example, CO_2 in MOFs is valuable because there are testable theoretical and computational relations between the self-diffusivity D_s and the Maxwell−Stefan diffusivity, $D_{T_{MS}}$, that are used to relate the molar flux of adsorbed molecules to the chemical potential gradient or "adsorptive driving force".[41−43]

Pulsed field gradient NMR (PFG-NMR, or diffusometry) is a well-established methodology used to measure directly the self-diffusion coefficient of adsorbed molecules in porous media. NMR quantifies the self-diffusivity by applying a linearly varied magnetic field in space, or "gradient pulse", serving to trace the probability of a molecule experiencing a displacement in space. This displacement is determined by the gradient pulse details and is typically on the order of micrometers−nanometers and is in the direction of the applied gradient field during a set experimental time, Δ, that is, diffusion time. The experiment is accomplished by applying pulses with sequentially varying gradient strength to sample the fraction of molecules experiencing the probability of a displacement. The effect on the NMR signal is manifest as a signal attenuation that may be Fourier-transformed to yield the spatial displacement propagator for the experimentally set diffusion time Δ. It is this relationship that enables PFG NMR methods to quantify the mean squared displacement MSD and thus the self-diffusion coefficient, $D_s = \frac{\mathrm{MSD}}{\Delta}$, where there is a dimensionality for the determination of the values.[44] When the gradient is applied along multiple axes with respect to the large laboratory NMR magnet, a self-diffusivity tensor may be determined.[45] Diffusometry techniques were previously transformative in the understanding of the motion of ad molecules in zeolitic materials. The methods developed previously have been extended to observe the diffusivity of adsorbed CO_2 in MOFs.[46] The measurement of the self-diffusivity is particularly insightful for direct comparison with diffusivities calculated from molecular dynamics simulations of the same systems and may eventually be used to predict macroscopic behavior.[47,48]

2. STUDIES OF MOLECULAR REORIENTATION THROUGH CSA

2.1. Open Metal Site Centered Reorientation

Open metal site MOFs are a subclass of coordination materials that possesses stable, under-coordinated metal ions after evacuation and/or activation, which may strongly interact with adsorbed molecules. Pioneering efforts to demonstrate the use of CSA analysis in open-metal site were first implemented

DOI: 10.1021/acs.chemrev.7b00695
Chem. Rev. 2018, 118, 10033−10048

in 2012[49] where the authors studied the Mg analogue of the isoreticular framework, Mg_2dobdc = 2,5-dihydroxyterephthalic acid (Mg_2(dobdc)), commonly referred to as Mg-MOF-74. The honeycomb structured framework (Figure 4) has been

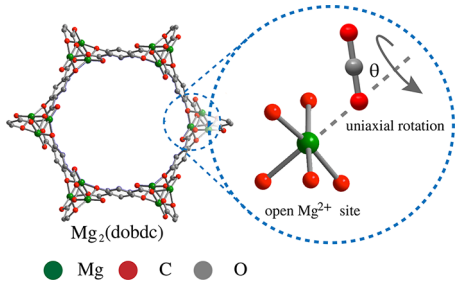

Figure 4. Schematic representing the structure of Mg_2(dobdc), MOF-74. The inset shows the open metal coordination site, along with a cartoon of CO_2 binding. Note θ depicts uniaxial rotation.

shown to have a greater capacity for CO_2 than most other MOFs at moderate processing conditions.[3] The authors established some precedents for the analytical treatment of CO_2 chemical shift powder patterns in the crystal framework of MOF. An accurate model that fits the data assumed a linear CO_2 molecule and oriented the PAS of the molecule along the metal-atom−oxygen bond axis, as shown in Figure 2, where the open-metal site was identified as the primary adsorption site. Second, they introduced the concept of uniaxial rotation, Figure 4, or tethering of one end of the CO_2 to the adsorption site and showed that varying the angle, α, could enable the fitting of a wide range of temperature-dependent CSA patterns. In their initial analysis, the angle theta decreases with increasing temperature, indicating (counterintuitively) that the rotating CO_2 occupies less phase space with increasing temperature. An article[50] demonstrated the complexity involved in the interpretation of CSA patterns by considering a helical hopping motion, as opposed to a uniaxial rotation, could be derived from molecular simulations (Monte Carlo and molecular dynamics). In this systematic study, the authors were the first to postulate and prove the contributions of localized and nonlocalized motion of the CO_2 in this MOF, where the helical distribution of metal adsorption sites led to the faux uniaxial rotation model. This insight highlights how the pairing of MD simulation with NMR experimental results facilitates greater understanding of complex MOF−adsorbate systems. This example also showed that the cumulative contributions from variable motional frequencies, rotating and hopping, may cumulatively contribute to the observed powdered pattern. Combined MC/MD and line shape analysis provided sufficient experimental and theoretical evidence to discern the primary trajectories sampled by CO_2 adsorbed in this MOF system.

This same MOF structure was studied in its pure and mixed metal form where the authors substituted 23% of the magnesium metal for cadmium, $Mg_{0.77}Cd_{0.23}$-MOF-74.[51] The first example of a "mixed" metal investigation in any MOF system will be discussed in more detail later. Here, we note that the authors analyzed the temperature dependence, loading dependence, and metal composition dependence of the ^{13}C CO_2 line shape coupled with DFT {density functional theory} computations to reveal the different types of CO_2 binding. The authors reintroduce a line width-weighted description of the CO_2 spectra with the following equation:

$$\Delta\sigma_{\text{eff}} = \Delta P_2[\cos\theta] = \Delta\left(\frac{3\cos^2\theta - 1}{2}\right) \quad (3)$$

where the variable P_2 is the second-order Legendre polynomial that incorporates both line width and sign into the observed chemical shift pattern. Here, the authors investigated higher loadings (0.8−1.15) of CO_2 per metal than was previously studied. This led them to discover a secondary adsorption site with an equivalent uniaxial rotation angle of 28°, whereas the primary adsorption site exhibited an equivalent angle of 68°.

2.2. Employment of Nonmetal Centered Crystal Frame for Orientation-Dependent Studies in Flexible MOFs

Although MOFs were originally cartooned as rigid porous media, the idea of flexible MOFs was introduced by the observation that, under certain thermodynamic conditions (temperature or adsorbate loading), a conformation change took place such that the pore size and/or shape changed; that is, the structural lattice "breathes" with changing adsorption conditions. One archetype of the flexible MOF is the MIL(Materials of the Institute Lavoisier)-53 series. Octahedral coordination of the metal oxide to bdc = 1−4-benzendicarboxylate (BDC) ligands yields a framework wherein a hydroxyl functional group serves as a bridge between the ligands to form a rhombic lattice with 0.85 nm × 0.85 nm 1-D channels (Figure 5) in the open configuration. In the narrow pore

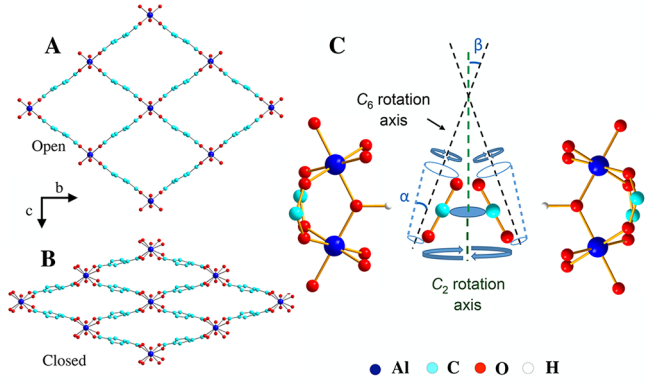

Figure 5. Schematic representing the open (A) and closed (B) configurations of the MIL-53 series and the rotational axes and angles in respect to the MOF pore used to model CO_2 motion.[54]

configuration, the channels are 0.26 nm × 1.36 nm. The MIL-53 series exhibits step adsorption isotherms, which make them attractive frameworks for both temperature- and pressure-swing applications.[52] The MIL-53 (Al, Ga) frameworks have shown a similar change in CO_2 capacity from the narrow pore state, holding 10 wt %, at 1 bar and 298 K, while the open pore state can adsorb 30 wt %, at 25 bar and 304 K.[53] The Ga analogue transitions from the narrow pore configuration to the open pore configuration state at slightly higher temperatures and pressures in comparison to the Al. The adsorption site location in the MOFs has not been experimentally located by traditional techniques, but computational studies suggest that the hydroxyl groups participate in the metal−oxygen hydrogen bonding. SSNMR experiments[54] were carried out to collect static ^{13}C powder patterns while the temperature was used to trigger conformational changes of the MOF at high and low loadings of CO_2 in MIL-53 (Al, Ga) and their amino-functionalized analogs. EXPRESS software was used to fit the

DOI: 10.1021/acs.chemrev.7b00695
Chem. Rev. 2018, 118, 10033−10048

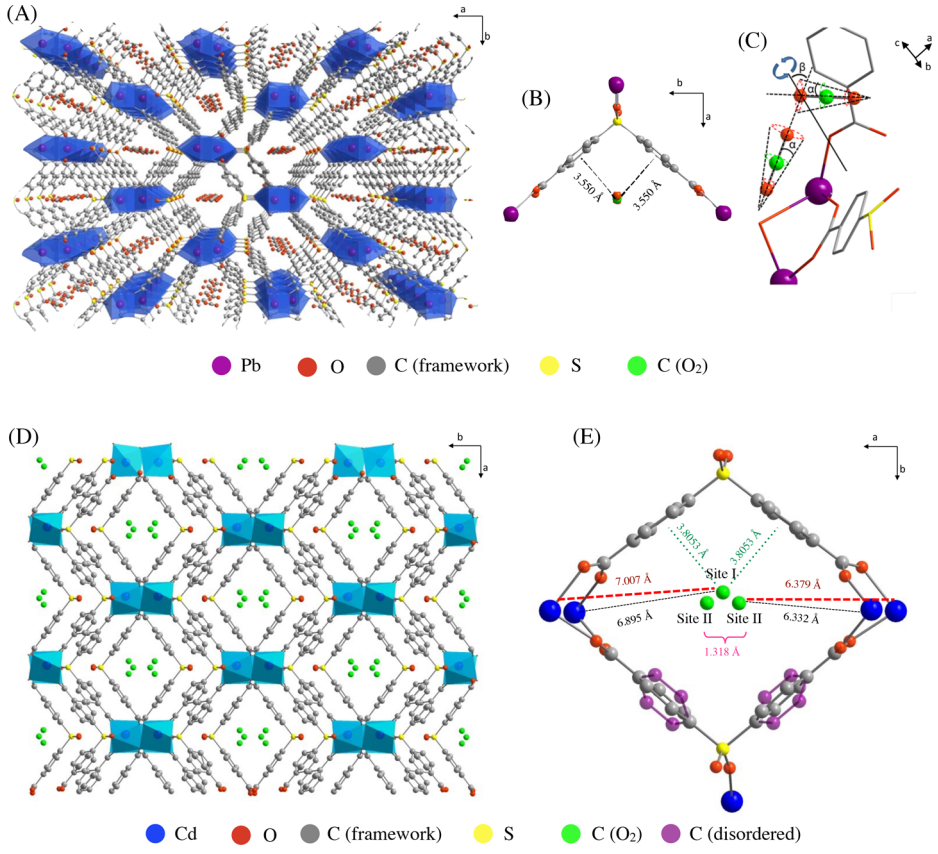

Figure 6. Schematic of CO_2 adsorbed in the Pb (A) and Cd (D) analogues of the SDB MOFs. A close-up view of the CO_2 adsorbed in the π-pockets (B) and the angular description (C), as well as CO_2 adsorbed in the Cd pockets (E). Adapted with permission from ref 57. Copyright 2016 American Chemical Society.

pattern and demonstrated that the adsorbed CO_2 experienced two modes of motion: rotation about the C_6 axis located at the hydroxyl groups and rotation about the C_2 axis associated with nonlocalized hopping between separate binding sites. The angle associated with these types of motion is affected by the metal site and can be visualized in Figure 5.

In comparison to the Al analogues, the Ga analogues exhibited smaller magnitudes of Ω and κ (Figure 1), but larger values of θ associated with the C_2 and C_6 axes of rotation. This implied that sampled configurational space of CO_2 in the Ga sample is larger in both the narrow pore and the open pore states, or simply that the CO_2 molecules experience weaker binding in the Ga analogue. These data correlate with the lower heat(s) of adsorption observed for CO_2 in the Ga framework.

The authors employed a clever use of cross-polarization to determine the location of the primary CO_2 adsorption sites. By decreasing the sample temperature and slowing the dynamic motion, the dipole−dipole interaction between the ^{13}C in CO_2 and adjacent protons becomes significant, enabling the use of cross-polarization to affect ^{13}C signal intensity. The authors substituted the protons on the hydroxyl group for deuterium in the MOF framework and found that they eliminated the ($^1H-^{13}C$) cross-polarization signal, confirming the spatial proximity of hydroxyl protons to adsorbed CO_2.

The cross-polarization transfer between the CO_2 carbon and the MOF-protons was used to infer the strength of the heteronuclear dipolar coupling. This strength is a proxy for the average distance between the two observed spins. The authors found that in the Ga analogue, the dipolar coupling was weaker between the carbon on the CO_2 and the protons on the framework, representative of longer proton-carbon averaged distances, suggesting that even though Ga has a narrow pore configuration, the CO_2 is not bound as tightly to the adsorption site, possibly due to the larger atomic radius of Ga as compared to Al. This is a unique example whereby SSNMR techniques identify the location of the primary adsorption site and used the dipolar coupling strength as a probe for proximity. In the amine-functionalized analogues of these MOFs, the CO_2 molecules were found to bind more strongly. Although previous studies indicated that the amino group does not serve as a binding site, the authors concluded that it enhances binding to the primary adsorption site.[55]

Investigators recently introduced a novel subclass of MOFs derived from the use of the V-shape ligand 4,4′-sulfonyldibenzoic acid (SDB) and the metal ions (Pb, Cd, Zn, Ca). Although the structure and the angle of the O−metal−O bond changes with the choice of metal, these MOFs are nevertheless loosely classified as an isoreticular framework series. They possess 1-D channels with one larger rhombic pore channel along the axis of the metal clusters surrounded by smaller channels of parallelograms.[56] This series lacks polarizing functional groups that most MOFs use to increase CO_2 adsorption affinity. Instead, their channels provide small physical π-pockets established by the proximity of the conjugated orbitals of the linkers, wherein CO_2 may adsorb. The location of CO_2 adsorption sites in the PbSDB and CdSDB frameworks had been examined by SCXRD (single crystal X-ray diffraction), yet Chen et al. engaged in an investigation[57] employing $^{13}CO_2$ SSNMR to explore the

DOI: 10.1021/acs.chemrev.7b00695
Chem. Rev. 2018, 118, 10033−10048

differences in adsorption dynamics (molecule orientation and jumping frequency) at low loadings between the PbSDB framework, which has linear shaped 1-D channels, and the CdSDB framework, which has sinusoidal shaped 1-D channels.

This work is an excellent example of the use of EXPRESS in calculating the chemical shift powder pattern subject to various types of motions. Briefly, the authors calculated the Herzfeld–Berger parameters for a single CO_2 associated with a single site, and then employed EXPRESS to discern CO_2 motion by careful fitting of model shift patterns with experimental data. The result is a surprisingly sophisticated view of the CO_2 dynamics wherein the adsorbed CO_2 rotates (or "wobbles") at an angle α (see Figure 6B), yet also hops between two equivalent sites characterized by an angle β (Figure 6B). The center point around which the molecules hop is not the metal center, but rather the π-pockets.

Finally, the authors enabled the simulations of flexible MOF systems by allowing the angle between the adjacently bonded linkers (the characteristic V of the rhombus) to vary during the fitting procedure. They were able to determine that PbSDB exhibited only one type of adsorption site described by the above-mentioned dynamics, while CdSDB with the shaped or sinusoidal channels exhibits two local CO_2 sites at both a symmetric and an antisymmetric π-pocket located further down the channel; the latter is present due to disorder in the arrangement of phenyl linkers in CdSDB.[58]

3. LOCATION DISCERNMENT AND EXCHANGE DYNAMICS

3.1. CO_2 in $Cu_3(BTC)_3$

Researchers[59] introduced an open metal site MOF Cu_3(btc) = 3·1,3,5-benzene tricarboxylate ($Cu_3(BTC)_3$) with a structure that consists of three types of isotropic pores connected by small windows. These pore domains are characterized as having the largest pore (0.9 nm) being surrounded by the middle pore (0.5 nm) and a small triangular pore (0.3 nm) that serves as the connecting window between the middle and large pore. Since its introduction as one of the first open-metal site MOFs (located in the large pore as shown in Figure 7),

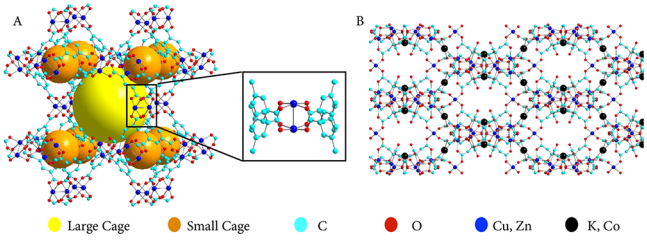

Figure 7. A structural schematics of the MOFs $Cu_3(BTC)_3$ (A) and UTSA-16 (B), where the ball colors of light blue, red, dark blue, and black represent the C, O, Cu or Zn, and K or Co, respectively. The guest molecules and hydrogen are omitted for visual clarity. On the left (A) are included a zoom-in of the open metal site as well as yellow and orange balls representing the large and small cage volumes native to the $Cu_3(BTC)_3$ structure.

investigators have explored the affinity of the undercoordinated Cu sites for CO_2 and CO. Crystallographic techniques have identified the primary adsorption sites at low loading (1 CO_2 per Cu site) to be located near the exposed metal, and secondary sites at higher loadings (1.5 CO_2 per Cu site) located near the window of the cages[60] due to CO_2 intermolecular interactions. Curiously, the measured adsorption enthalpy remains unchanged during the transition between higher and lower loadings. The D_s and T_1 of CO_2 in $Cu_3(BTC)_3$ were first quantified at varying pressures in 2012 (Figure 7).[61] The authors provided no significant insights about the mechanism driving the dynamic behavior of CO_2, but rather focused on the comparison of CO_2 and CH_4 diffusive motions. As such, this work is the first measurement of the D_s in an open-metal site MOF.

In 2013, Gul-E-Nor et al.[62] investigated the role that the metal ion plays in CO_2 and CO adsorptive behavior in the parent MOF $Cu_3(BTC)_3$ by doping zinc into the framework, $Cu_{2.977}Zn_{0.03}(BTC)_3$. The authors demonstrated the sensitivity of the adsorbed spectra of ^{13}CO to the surrounding or local MOF electronic environment. SSNMR in systems containing paramagnetic metals are complicated by the presence of interactions between nuclei and the very strong magnetic moments of unpaired electrons. These interactions produce broadening and very large shifts. The changing magnitude of broadening and shifts with metal loading is a qualitative measure, then, of electron–nuclear interactions. The authors recorded δ_{iso} as a function of temperature to track the interactions of CO_2 with the Cu^{2+} $S = 1/2$ electronic state. A follow-up publication quantified the spin–lattice relaxation rates were used to explore the heterogeneous states of the adsorbed phases contributing separately to local motion.[63] This relaxation analysis is informative as it provides a deep analysis of the fluctuating fields that give rise to a relaxation rate maximum. Surprisingly, it is not the fluctuating fields from unpaired electrons; rather, it is jump motion that was fully determined in this insightful analysis.

3.2. CO_2 in UTSA-16

The anatase-like structure of MOF UTSA-16 (K-$(H_2O)_2Co_3(cit)_2$), where cit = citrate, was first investigated for magnetic applications.[64] Later, in 2012 Xiang[65] et al. investigated its affinity for CO_2 and found that the diamondoid cages with 0.45 nm edges serve to efficiently trap CO_2 molecules, while the 0.33 nm × 0.55 nm connecting windows served to select CO_2 over other gases by size discrimination. UTSA-16 is stable in the presence of H_2O, and it is postulated that this stability enhances the CO_2 adsorption through hydrogen-bonding interactions. In a later study, investigators concluded that, although the K^+ ion site serves as the primary adsorption site for CO_2, 22% of the CO_2 adsorbed is not explained by the observed enthalpy of adsorption to this cation. Masala[66] et al. employed SSNMR as a complementary technique to investigate this unexplained fraction and found that, in addition to the expected spectra associated with the K^+ sites, additional adsorption sites displayed distinct chemical shift differences in the static spectra and then determined this site to be present because of favorable ligand interactions. Exchange rates between the sites were probed using variable-temperature experiments, where the authors concluded that the activation energy for exchange between the primary (metal) and secondary adsorption (ligand) site was in the range of 6.3–9.3 kJ/mol. They also found the line width associated with the CO_2 spectra to be greater than 1 kHz, meaning that the CO_2 species is experiencing reduced motional freedom.

DOI: 10.1021/acs.chemrev.7b00695
Chem. Rev. 2018, 118, 10033–10048

4. DIRECT PROBES OF TRANSLATIONAL AND ROTATIONAL MOTION

4.1. CO_2 Loading Dependence

Zeolitic imidozolate frameworks (ZIFs) are a series of MOFs that actualize topologies similar to known zeolites due to the bridging angle inherent to the imidazole organic linker. The zinc 2-methyl-imidazolate $Zn(MeIM)_2$ (ZIF-8)) framework has the sodalite zeolite structure with a larger diameter cavity of pore 1.16 nm × 0.36 nm connecting windows. ZIF-8 is considered an isotropic MOF due to its cubic SOD-like symmetry. Along with other zeolitic imidozolate frameworks (ZIF), ZIF-8 was initially well-known for its thermal and chemical stability. More recently, Liu[67] et al. demonstrated that after long exposure (7+ days) to an H_2O and CO_2 slurry, the structure irreversibly degrades to a zinc−carbonate-based powder. Many early investigators explored ZIF-8 for use in both postcombustion carbon capture and (more recently) natural gas enrichment, resulting in a thorough characterization that has enabled large-scale production and successful incorporation into composite polymer membranes. Diaz[48] et al. investigated the apparent self-diffusivity of CO_2 in polysulfone-ZIF-8 mixed matrix membranes via PFG NMR. This work demonstrated the gas diffusivity was enhanced with increasing weight fraction of ZIF-8, but could not parse this enhanced diffusivity from that associated with the void space at the polymer−filler interface and partial occupation of the ZIF-8 by polymer chains.

Pusch[68] et al. presented ZIF-8 as a model moderate-interacting system to investigate the dependence of the translation motion of CO_2 and CH_4 on adsorbate loading with NMR diffusometry methods. After preparation of samples through a common flame-sealing technique, the authors indicated that they observed multiexponential signal decay, or multiple D_s coefficients, at all pressures (7−15 bar) at room temperature. The authors chose to associate the slowest CO_2 self-diffusion coefficient with diffusion in the intracrystalline regime, while the faster self-diffusion coefficient sampled both the intra- and intercrystalline environments. Tracking the intracrystalline D_s, the authors showed that translational motion in the ZIF-8-CO_2 did not vary with increasing loading. Although the pores were expected to produce more intramolecular collisions (the kinetic diameter of CO_2 (0.33 nm) is smaller than that of the pore windows in the framework), the translational motion of CO_2 is not inhibited by sieving effects or travel through these windows.

As of this writing, high-pressure CO_2 adsorption isotherms were not available. In 2013, however, Liu[69] et al. were able to quantify CO_2 adsorption in the high-pressure regime (1−30 bar) and found that CO_2 loadings were much lower than previously predicted (6−7 molecules/cage) and contributions from intermolecular drag forces to diffusion would actually be negligible.

4.2. Unique Insight of Anisotropic CO_2 Motion by Combining CSA and Axial Specific PFG Methods

DMOF-1 is a prototypic pillared MOF structure investigated for CO_2 adsorption by many experimental and computational techniques that consists of zinc oxide clusters and 1−4-benzendicarboxylate, DABCO = diazabicyclo-octane ligands (Figure 8). This literature indicates that the substitution of the pillared ligands (DABCO) may increase favorable adsorbate−adsorbent interactions. Although DMOF-1 and derivatives exhibit a cubic center structure similar to that of IRMOF-1, the

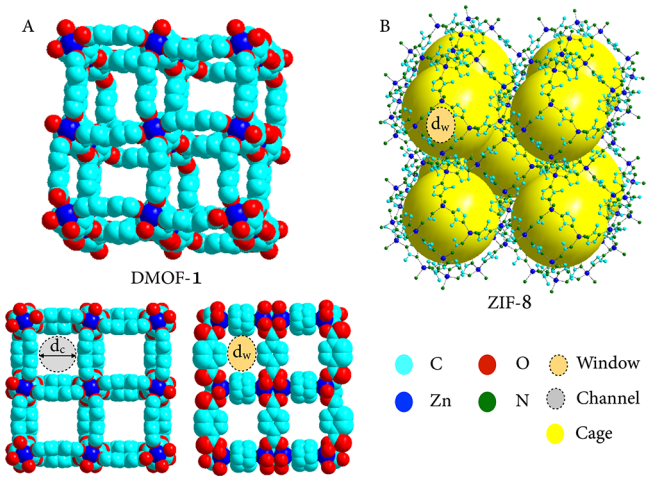

Figure 8. Structural schematics of the MOFs $Zn_2(BDC)_2DABCO$ (BDC = 1,4-benzendicarboxylate, DABCO = diazabicyclo-octane) (DMOF-1) (A) and ZIF-8 (B) where the ball colors of light blue, red, dark blue, and black represent the C, O, Cu or Zn, and K or Co, respectively. The guest molecules and hydrogen are omitted for visual clarity. On the left (A) are included a zoom of the open metal site as well as yellow and orange balls representing the large and small cage volumes native to the $Cu_3(BTC)_3$ structure.

substitution of a pillared linker creates a unique anisotropic pore environment and introduces two pore sizes: larger pores sized at 0.75 nm and a small window of 0.4 nm. An early investigation that combined molecular simulations and experiment[70] demonstrated a contrary trend for increasing low-pressure CO_2 affinity through the functionalization of the connecting ligand with nonpolar groups. Thus, DMOF-1 is a model pillared-type MOF that affords investigation of unusual MOF−guest interactions of CO_2 created by an anisotropic nonpolar chemical environment apportioned onto an isotropic structural environment. SSNMR techniques are ideal for determining how the anisotropic chemical environments could contribute to anisotropic motion and adsorbate location in this type of MOF. Peska[71] et al. found that the anisotropic motion contributes to the CSA powder pattern in DMOF-1 and is manifest by directionally dependent self-diffusion. The authors demonstrated that the axially symmetric residual chemical shift tensor, $\Delta\delta = \delta_{\parallel} - \delta\perp$, which contains components from either the channel or the window direction with respect to the crystal frame, could be used in conjunction with SIMPSON simulations to confirm the preferential orientation of CO_2 along one of the channels of DMOF-1. The adsorption sites were characterized previously to be located near the zinc cluster and a less favorable site proximate to the benzene rings. They determined the trace components of the diffusion tensor, $Tr(\vec{D}) = \frac{D_{\parallel} + D_{\perp}}{3}$, and the resulting degree of diffusional anisotropy, $\eta = \frac{D_{\parallel}}{D_{\perp}}$, from axial-specific pulsed field gradient NMR.

These results demonstrate that, depending on the degree of anisotropy, the observed chemical shift powder pattern spectra may decay nonuniformly with the application of pulsed field gradients. In the present case, those CO_2 molecules diffusing along the channel direction in the MOF crystallites are moving in a channel aligned with the applied gradients. When the gradient was applied in directions not aligned with the 1-D channels, the D_s for crossing between channels was much

DOI: 10.1021/acs.chemrev.7b00695
Chem. Rev. 2018, 118, 10033−10048

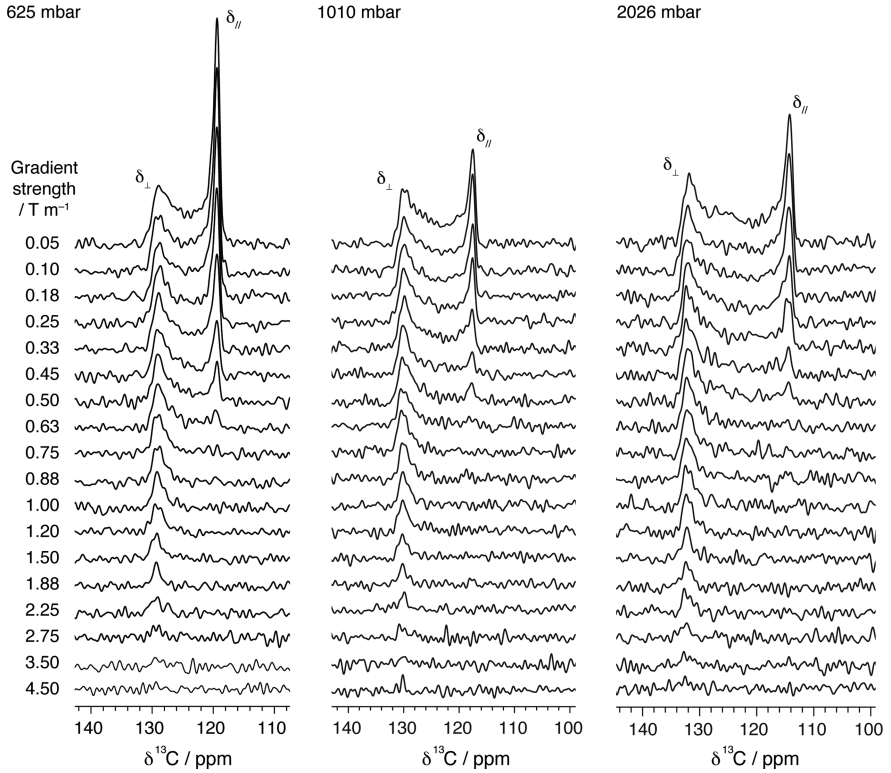

Figure 9. Diffusive attenuation of the CO_2 powder patterns with increasing magnitude of the applied z-gradient at various loadings of CO_2 adsorbed in large crystallites of MOF-74(Zn) with increasing loading (left to right). The chemical shift intensity associated with the CO_2 molecules parallel to the direction of the applied gradient, $\delta_{||}$, decays at faster rates than the chemical shift intensity associated with CO_2 traveling perpendicular to the channels, $\delta_{\perp}$.

slower. CSA patterns facilitated the conclusion that the CO_2 molecules traveled with the O═C═O vector primarily orientated parallel to, and moving in the direction of, 1-D channels in DMOF-1. The preferential orientation and the diffusion of the CO_2 molecules along the channels allowed the authors to conclude that the pillars in this framework provide a series of moderately strong adsorption sites that direct the diffusion of molecules. This conclusion was reached by application of multiaxis PFG NMR methods, an established microscopic technique that quantifies the intracrystalline diffusion tensor. Similar conclusions[72] can be reached if crystallites are macroscopically ordered in the direction of the applied laboratory field. These authors applied this method to demonstrate the loading dependence of the self-diffusion along the direction of MOF-74(Zn) channels and paired their result with loading-dependent self-diffusivities calculated from MD simulations (Figure 9).

In situ NMR revealed[73] the variations of NMR observables due to varying the thermodynamics state of CO_2 in Zn_2(BME-bdc)$_x$(db-bdc)$_{2x}$dabco (x = 2, 1.5, 1, 0.5, 0) (BME-bdc = 2,5-bis(2-methoxy)-1,4-benzenedicarboxylate and dabco = 1,4-diazabicyclo[2,2,2]octane), a breathing derivative of the pillared MOF DMOF-1. These experiments demonstrated the first use of an in situ gas dosing apparatus to quantify adsorption and desorption of CO_2, thereby adding a new capability to the NMR toolbox. They also demonstrated the use of the chemical shift power pattern to identify the transition of a breathing MOF from its narrow pore to large pore configurations. Paired with the careful implementation of 2D-exchange NMR, a coveted multidimensional NMR technique that enables monitoring of millisecond time scale exchange, the rate of motion of a molecule moving from one local type pore geometry to another was quantified. The authors concluded that the exchange rate between CO_2 molecules at strong adsorption sites and freely moving CO_2 molecules in local areas in the MOF was slow. Although the adsorption enthalpies of CO_2 in the MOFs are relatively low, the adsorption sites present in this MOF create a physical pocket that immobilizes the CO_2 molecules. Other techniques to study adsorption dynamics do not have the necessary temporal resolution to reveal such exchange processes.

4.3. Discerning Molecular Correlation Times

The first measurement of molecular correlation times for CO_2 adsorbed in an metal organic framework employed R_1 measurements from CO_2 in Mg_2(dobdc).[49] The fluctuating magnetic fields that give rise to the relaxation, with their attendant correlation times, were assumed to derive from the CSA and nuclear dipole−dipole interactions. The authors BPP theory to derive the thermal activation energies for motional correlation times, and in so doing discovered that there are two correlation times associated with different activation energies for the low and moderate loadings of the Mg_2(dobdc) analogue. Fluctuating magnetic fields due to the heteronuclear $^1H-^{13}C$ dipolar coupling dominated the apparent relaxation rates. Although there were two activated processes observed, the correlation times could not be assigned to a particular type of motion.

Relaxation rates for CO_2 in ZIF-8 systems[74] determined the effect of loading or gas density (ρ) on the longitudinal relaxation rate (R_1) through quantification of the "surface relaxivity" of CO_2 in ZIF-8. Although methane in this system exhibited a linear dependence of R_1 on the density of the

DOI: 10.1021/acs.chemrev.7b00695
Chem. Rev. 2018, 118, 10033−10048

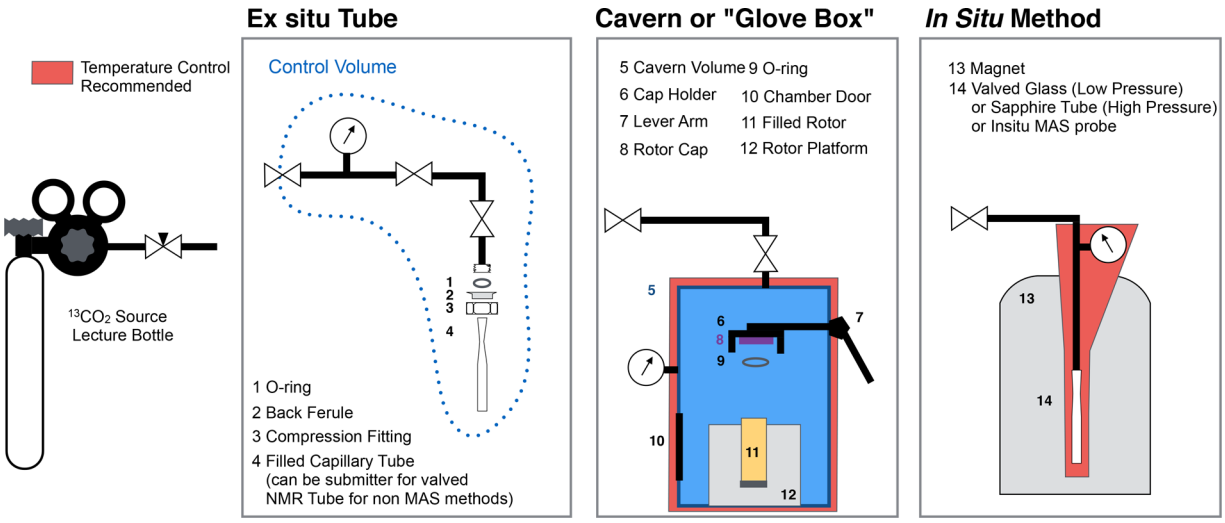

Figure 10. Recommended experimental equipment for both ex situ and in situ methods that enables better control of the thermodynamic state.

adsorbed phase (loading), to describe the relationship with CO_2, the Enskog correction[75] for adsorbed phase density was necessary for interpretation of the data. The Enskog correction accounts for the interactions that take place between pure gaseous molecules at higher densities (pressures) explicitly when the molecular diameter is on the order of the average intermolecular distance of the gases. This correction has only been found to be valid for R_1 correlated with low-to-moderate densities of CO_2 where intermolecular collisions are still dominating the reorientation rates of the molecules. The surface relaxivity arising from loading-dependent measurements[74] may be used to quantify the adsorbate−adsorbent interaction of gases in MOFs. In a follow-up article, these same authors used R_1 measurements to determine the local jump dynamics of CO_2 in $Cu_3(BTC)_3$. They calculated the average jump length of the adsorbed molecules from the local motion correlation time determined by the minimum T_1 with respect to gas density. They further concluded that this jump length was greater than the distance between the neighboring adsorption sites that were previously reported.[76] This indicated that the CO and CO_2 molecules exchange primarily with other molecules adsorbed in the lattice and not from site-to-site once adsorbed. These SSNMR analyses enabled a new finding that was not obvious from traditional characterization of the location of the adsorption sites or of their adsorption enthalpies. A summary of CO_2 CSA values from the literature has been included in the Supporting Information.

5. OPPORTUNITIES

The experimental and thermodynamic complexities associated with CO_2 adsorption on MOFs have led to many experimental challenges, yet also afford the design and implementation of SSNMR experimental and analytical methods. This section exhorts the community to adopt a more standardized approach for the preparation of samples so as to lead to increased reproducibility between researchers, as well as enable a wide range of experimental methods to access the necessary thermodynamic states.

5.1. Challenge of Controlling Thermodynamic State

It is first important to acknowledge the necessity of experimentally controlling thermodynamic conditions for gas adsorption in metal−organic frameworks. In particular, MOFs have shown state-dependent performance and dynamic behavior that influences strongly the observed host−guest interactions. To truly develop a molecular understanding of adsorbate motion, location, and interactions, the experimental practitioner must be able to place their experimental conditions on the adsorption isotherm observed for the particular MOF−gas systems, essentially recording its thermodynamic state. In so doing, the derived experimental parameters may be directly compared to molecular simulations. Further, as the magnetic resonance community seeks to reproduce and compare data from one group to the other, we should understand the limitations that certain sample preparation methods have on our ability to deduce conclusions from NMR observables. Thus, this section will summarize and suggest the practical ways for laboratories with different amounts of funding to access this information.

One of the most common methods for gas-dosing porous adsorbents in NMR studies is a process that involves flame sealing a capillary tube. This is most common because it is the least expensive dosing methodology and derives from the early days of NMR studies of chemisorbed gases[40] and is executed apart from the execution of NMR experiment, or ex situ. This technique is useful when adsorption isotherms for CO_2 have been measured at room and/or liquid nitrogen temperatures. We recommend an apparatus that follows the ex situ dosing schematic shown in Figure 10. The apparatus should be designed so that the free volume of the area enclosed by the dashed line is well-defined. Initially, the weight of the activated MOF and the glass tube should be recorded and then brought to an equilibrium pressure at a uniform temperature throughout the apparatus piping. We recommend that a compression fitting with a temperature resistant O-ring be used to seal the glass capillary to the metal fixture, as shown in the schematic. After reaching an equilibrium pressure, the gas source should be isolated from the gauge by closing a valve, thus ensuring a known nonadsorbed volume of CO_2 associated with the displayed pressure, as well as a known amount of free CO_2 in the headspace of the capillary tube; this pressure should be recorded. The bottom of the capillary glass tube is dipped in liquid nitrogen and sealed with the oxygen-gas fueled flame. After the tube is sealed, the new displayed pressure in the control volume should be recorded, and the loss of CO_2 to the capillary tube may be estimated. The advantage of this

DOI: 10.1021/acs.chemrev.7b00695
Chem. Rev. 2018, 118, 10033−10048

technique is that the material cost of the apparatus is affordable to most research laboratories; however, it is important to understand the uncertainty in the estimated loading. Although cryo-pumping achieves subatmosphere pressures facilitating flame-sealing, it results in a higher pressure in the sealed capillary tube and the remaining head−head space than the equilibrium loading determined by adsorption isotherms. Although mass change can be estimated by weighing the capillary tube before and after, the added weight of the CO_2 is not easily detectable by most mass scale(s). Most importantly, any variation in the temperature of the sample will cause variation in the actual adsorbed amount of CO_2; this is difficult to determine because the total pressure inside the NMR tube is unknown. Although researchers have attempted to track the adsorbed amount with quantitative NMR methods, this is only successful if the adsorbed gas molecule has a distinctive chemical shift from the free gas in the tube, and the head space is well-defined inside the RF coil. Another ex situ dosing method requires the use of valved NMR tubes purchasable from glass manufacturers for reasonable prices. We recommend purchasing one with a compression fitting that allows for easy exchange from the sealing apparatus. The sample should be properly evacuated, brought to the same pressure and temperature condition(s) as the planned NMR experiment, and allowed to reach equilibrium. Next, the valve should be closed and brought to ambient conditions before inserting the sample in the magnet. The advantage of this ex situ dosing method is that it allows the researcher a high degree of precision in matching the conditions of an adsorption isotherm. The disadvantage of the technique is that it requires the researcher to use a NMR probe that will accept the geometry of a long glass tube. Most SSNMR probes have a geometry that is not compatible with long glass tubes.

SSNMR experiments that require magic angle spinning have been accessed experimentally by placing a flame-sealed capillary tube inside the rotors and then spinning with caution to avoid a rotor explosion or rotor failure. Another ex situ dosing option is the use of a CO_2 "glove box" or cavern method[77] for sample preparation, as it provides the most ideal loading environment for samples requiring MAS. It is recommended that a rotor with a gastight cap, normally accompanied by sealing O-ring (e.g., Bruker) rotors, or a sealing cell insert (e.g., Doty rotors), should be used. If the rotor is not gastight, it is possible for the CO_2 leak to the atmosphere. In this approach, the MAS rotor is loaded with the activated MOF, and placed under vacuum onto a stabilizing stage inside a small cavern, as shown in Figure 10, equipped with a vacuum pump, as gas in flow, and a mechanical lever operated from outside the chamber enabling the capping of either the sealing cell or the rotor without disturbing the cavern pressure. The cavern atmospheric pressure, gas composition, and temperature may be controlled to define the pressure at which the MOF was loaded and sealed. The advantage of this ex situ method is that the researcher may match the condition of experimentally determine adsorption isotherms. The disadvantage of this method is that the apparatus is more costly to have machined and may potentially waste a significant amount of expense on isotopically enriched gas.

Another extremely useful sample preparation method is the in situ approach. This requires careful measurement of the down stream sample pressure and temperature in the presence of a strong magnetic field. Although complex, many groups have been able to construct specialized SSNMR probes[78] and a top-loading apparatus[79] that achieve true in situ operation. This method of study allows for the most accurate measurements of NMR observables and the thermodynamic state.

5.2. Advancing the Understanding of Adsorbed Species Relaxation

The use of relaxometry to understand adsorption dynamics in MOF is underutilized. We note that for every NMR experiment conducted with MOFs the relaxation parameters are typically quantified to determine the optimal experimental parameters, such as the delays associated with signal averaging. Yet this relaxation is rarely mentioned in published investigations. The barrier to reporting such data is that it opens a whole new avenue of interpretation, often requiring complex applications of molecular models, which are further complicated by the presence of framework. This is particularly true if quantifying a relaxation rate trend with respect to some change in the state of the adsorbent−adsorbate system (loading, temperature, time). Given the simple linear geometry of the CO_2 molecule, however, interpretation of powder chemical shift spectra constrains the types of molecular motion to be considered.

There are two principal questions that all investigators must ask to extract useful information from relaxation parameters: What is the "normal" relaxation behavior of pure CO_2, and what is the deviation from the normal behavior due to the confinement within a specific type of MOF? It is important to note that extensive work has been conducted by leaders in shale gas[80] and xenon NMR[81] research fields that can greatly benefit the interpretation of relaxometry data of CO_2 and other gases. We have found these references to be particularly helpful: *Gas Phase NMR* edited by Karol Jackowski and Micha Jaszuski (2016) contains many useful chapters; a basic introduction to models that describe the molecular reorientation of gases is found in ref 38; in ref 75 the investigators have conducted a number of experimental and theoretical studies and reviews that not are not specific to CO_2; and there is substantial shale gas literature published in the 20th century that establishes the basic behavior of CO_2 at various pressures and temperatures as a pure species[82] and within rocks.

5.3. Increasing Collaboration with Simulation Groups To Calculate NMR Observables

Because of its highly sensitive probe of local electronic structure and motion, NMR is uniquely suited to be paired with physical simulations of host−guest interactions. All NMR experiments assess how spin ensembles in specific states relax to equilibrium after a perturbation. That perturbation is due to a strategically selected pulse sequence that activates a pathway to nuclear spin excited states and controls the allowed avenues for relaxation. As demonstrated by the literature, the NMR community can span the necessary thermodynamic experimental space, as well as naturally sample a wide range of times scales (Hz−MHz), so as to compare with molecular dynamics simulations and first principle calculations of electronic structure (e.g., density functional theory (DFT) methods). The MolSim MOF community[83] has shown an enormous capacity for screening capacity, selectivities, and other performance criteria, as well as representing the details of molecular physics that influence host−guest interactions, yet suffers enormously from a lack of comparable experimental data directly sensitive to these physics. This community would benefit greatly from validation of these interaction forces (or

DOI: 10.1021/acs.chemrev.7b00695
Chem. Rev. 2018, 118, 10033−10048

force fields). The discernment of the complex hopping motion of CO_2 in Mg-MOF-74[84] illustrates well the synergism possible when combining simulation and theory.

ASSOCIATED CONTENT

Supporting Information

The Supporting Information is available free of charge on the ACS Publications website at DOI: 10.1021/acs.chemrev.7b00695.

Summary of the CSA values of $^{13}CO_2$ adsorbed in MOFs from the literature (PDF)

AUTHOR INFORMATION

Corresponding Author

*E-mail: reimer@berkeley.edu.

ORCID

Velencia J. Witherspoon: 0000-0002-2718-6605
Jun Xu: 0000-0003-3507-0159
Jeffrey A. Reimer: 0000-0002-4191-3725

Notes

The authors declare no competing financial interest.
This paper is an additional review for *Chem. Rev.* **2017**, volume *117*, issue 14 "Carbon Capture and Separation".

Biographies

Velencia J. Witherspoon received her B.S. in Chemical Engineering from Florida A&M University and later completed her Ph.D. at the UC Berkeley in 2017 under the tutelage of Prof. Jeffrey Reimer. There she developed NMR methodologies to understand the adsorptive behavior of small molecules in metal organic frameworks and was the recipient of the UC Chancellor's Doctoral Fellowship, the National Science Foundation Graduate Research Fellowship, and the ACalNet DAAD Fellowship, which sponsored her time at RWTH University (Germany), in the lab of Prof. Blmich. Most recently, she is a National Research Council Postdoctoral Fellow investigating dynamics in soft materials at the National Institutes of Standards and Technology in Gaithersburg, MD.

Jun Xu obtained his B.S. degrees from Peking University (China) in 2008 and completed his Ph.D. study under the supervision of Professor Yining Huang at the University of Western Ontario (Canada) in 2013. As a Postdoctoral Fellow, he joined Prof. Jeffrey A. Reimer's group at University of California, Berkeley in 2014 and then moved to Prof. Christophe Coperet's group at ETH Zurich (Switzerland) in 2017. Since September of 2018, he is an associate professor at Nankai University (China). His current research interests focus on the development of solid-state NMR methods for the characterization of rare-earth materials.

Jeffrey A. Reimer is the C. Judson King Endowed Professor and the Warren and Katharine Schlinger Distinguished Professor and Chair of the Chemical and Biomolecular Engineering Department at UC Berkeley. He is a Fellow of the American Association for the Advancement of Science, a Fellow of the American Physical Society in the Division of Materials Physics, a Fellow of the International Society for Magnetic Resonance, and the recipient of a Research Fellowship from the Alexander von Humboldt Foundation. In addition to his 190 research publications, Professor Reimer is coauthor (with T. M. Duncan) of the introductory text *Chemical Engineering Design and Analysis* (Cambridge University Press, 1998), and the text *Carbon Capture and Sequestration* (with Berend Smit, Curt Oldenburg, Ian Bourg, World Scientific Press, 2013).

ACKNOWLEDGMENTS

We are grateful for research support from the Center for Gas Separations Relevant to Clean Energy Technologies, an Energy Frontier Research Center funded by the U.S. Department of Energy, Office of Science, Basic Energy Sciences, under award DE-SC0001015. We acknowledge A. Forse for creating Figure 9.

REFERENCES

(1) Meek, S. T.; Greathouse, J. A.; Allendorf, M. D. Metal-organic frameworks: a rapidly growing class of versatile nanoporous materials. *Adv. Mater.* **2011**, *23*, 249−67.
(2) Zhang, Z.; Yao, Z.; Xiang, S.; Chen, B. Perspective of Microporous Metal-Organic Frameworks for CO_2 Capture and separation. *Energy Environ. Sci.* **2014**, *7*, 2868.
(3) Mason, J. A.; Sumida, K.; Herm, Z. R.; Krishna, R.; Long, J. R. Evaluating metal−organic frameworks for post-combustion carbon dioxide capture via temperature swing adsorption. *Energy Environ. Sci.* **2011**, *4*, 3030.
(4) Sumida, K.; Rogow, D. L.; Mason, J. A.; McDonald, T. M.; Bloch, E. D.; Herm, Z. R.; Bae, T.-H.; Long, J. R. Carbon dioxide capture in metal-organic frameworks. *Chem. Rev.* **2012**, *112*, 724−81.
(5) Stock, N.; Biswas, S. Synthesis of metal-organic frameworks (MOFs): routes to various MOF topologies, morphologies, and composites. *Chem. Rev.* **2012**, *112*, 933−969.
(6) Li, J.-R.; Kuppler, R. J.; Zhou, H.-C. Selective gas adsorption and separation in metal-organic frameworks. *Chem. Soc. Rev.* **2009**, *38*, 1477−504.
(7) D'Alessandro, D. M.; Smit, B.; Long, J. R. Carbon dioxide capture: Prospects for new materials. *Angew. Chem., Int. Ed.* **2010**, *49*, 6058−6082.
(8) Werner, M.; Rothermel, N.; Breitzke, H.; Gutmann, T.; Buntkowsky, G. Recent Advances in Solid State NMR of Small Molecules in Confinement. *Isr. J. Chem.* **2014**, *54*, 60−73.
(9) Hoffmann, H. C.; Debowski, M.; Müller, P.; Paasch, S.; Senkovska, I.; Kaskel, S.; Brunner, E. Solid-state NMR spectroscopy of metal-organic framework compounds (MOFs). *Materials* **2012**, *5*, 2537−2572.
(10) Schaefer, D.; Favre, D. *J. Am. Chem. Soc.*
(11) VanderHart, D. L. Rigid-Lattice NMR Moments and Line Shapes with Chemical-Shift Anisotropy. *J. Chem. Phys.* **1968**, *49*, 261.
(12) Vold, R.; Hoatson, G. Effects of jump dynamics on solid state nuclear magnetic resonance line shapes and spin relaxation times. *J. Magn. Reson.* **2009**, *198*, 57−72.
(13) Duer, M. J. *Solid State NMR Spectroscopy: Principles and Applications*; John Wiley & Sons: New York, 2008.
(14) Barrie, P. Characterization of porous media using NMR methods. *Annu. Rep. NMR Spectrosc.* **2000**, *41*, 265−316.
(15) Ford, D. C.; Dubbeldam, D.; Snurr, R. Q.; Ku, V.; Wehring, M.; Stallmach, F.; Mu, U. Self-Diffusion of Chain Molecules in the Metal Organic Framework IRMOF-1: Simulation and Experiment. *J. Phys. Chem. Lett.* **2012**, *3*, 1−4.
(16) Abraham, R. J.; Fisher, J.; Loftus, P. *Introduction to NMR Spectroscopy*; Wiley: New York, 1988.
(17) Jameson, C. J. Chemical shift scales on an absolute basis. *eMagRes.* **2011**, 1 DOI: 10.1002/9780470034590.emrstm0072.pub2.
(18) Herzfeld, J.; Berger, A. E. Sideband intensities in NMR spectra of samples spinning at the magic angle. *J. Chem. Phys.* **1980**, *73*, 6021−6030.
(19) Orendt, A. M. Chemical Shift Tensor Measurement in Solids. *Encycl. Nucl. Magn. Reson.* **2003**, *9*, 1282−1296.
(20) Bloembergen, N.; Purcell, E.; Pound, R. Relaxation effects in nuclear magnetic resonance absorption. *Phys. Rev.* **1948**, *73*, 679.
(21) Spiess, H. Molecular Motion studied by NMR Powder Spectra 1.Lineshape caclulation for axially symmetric sheilding tensors. *Chem. Phys.* **1974**, *6*, 217−225.

DOI: 10.1021/acs.chemrev.7b00695
Chem. Rev. 2018, 118, 10033−10048

(22) Wasylishen, R. E.; Friedrich, J. O.; Mooibroek, S.; Macdonald, J. B. Spectra of carbon monoxide and carbon dioxide. *J. Chem. Phys.* **1985**, *83*, 548−551.
(23) Omi, H.; Ueda, T.; Miyakubo, K.; Eguchi, T. Dynamics of CO_2 Molecules Confined in the Micropores of Solids as Studied by ^{13}C NMR. *Appl. Surf. Sci.* **2005**, *252*, 660−667.
(24) Bak, M.; Rasmussen, J. T.; Nielsen, N. C. SIMPSON: a general simulation program for solid-state NMR spectroscopy. *J. Magn. Reson.* **2000**, *147*, 296−330.
(25) Bonhomme, C.; Gervais, C.; Laurencin, D. Recent NMR developments applied to organic−inorganic materials. *Prog. Nucl. Magn. Reson. Spectrosc.* **2014**, *77*, 1−48.
(26) Bain, A. D. Chemical exchange in NMR. *Prog. Nucl. Magn. Reson. Spectrosc.* **2003**, *43*, 63−103.
(27) Suwelack, D.; Rothwell, W.; Waugh, J. Slow molecular motion detected in the NMR spectra of rotating solids. *J. Chem. Phys.* **1980**, *73*, 2559−2569.
(28) Kimmich, R. Strange kinetics, porous media, and NMR. *Chem. Phys.* **2002**, *284*, 253−285.
(29) Pines, A.; Gibby, M.; Waugh, J. Proton-enhanced nuclear induction spectroscopy. A method for high resolution NMR of dilute spins in solids. *J. Chem. Phys.* **1972**, *56*, 1776−1777.
(30) Taylor, R. Setting up ^{13}C CP/MAS experiments. *Concepts Magn. Reson.* **2004**, *22A*, 37−49.
(31) Strange, J. H.; Mitchell, J.; Webber, J. B. W. Pore surface exploration by NMR. *Magn. Reson. Imaging* **2002**, *21*, 221−6.
(32) Gonzalez, J.; Nandini Devi, R.; Tunstall, D. P.; Cox, P. A.; Wright, P. A. Deuterium NMR studies of framework and guest mobility in the metal−organic framework compound MOF-5, $Zn_4O(O_2CC_6H_4CO_2)_3$. *Microporous Mesoporous Mater.* **2005**, *84*, 97−104.
(33) Ueda, T.; Kurokawa, K. ^1H NMR Study of Molecular Motion of Benzene and n-Decane Confined in the Nanocavities of Metal Organic Frameworks. *J. Phys. Chem. C* **2012**, *116*, 1012−1019.
(34) Kowalewski, J.; Maler, L. *Nuclear Spin Relaxation in Liquids: Theory, Experiments, and Applications*; CRC Press: New York, 2006.
(35) L. Sudmeier, J.; E. Anderson, S.; S. Frye, J. Calculation of Nuclear Spin Relaxation Times. *Concepts Magn. Reson.* **1990**, *2*, 197−212.
(36) Korb, J.; Xu, S.; Cros, F.; Malier, L.; Jonas, J.; Korb, J. Quenched molecular reorientation and angular momentum for liquids confined to nanopores of silica glasses. *J. Chem. Phys.* **1997**, *107*, 4044.
(37) D'Agostino, C.; Mitchell, J.; Mantle, M. D.; Gladden, L. F. Interpretation of NMR Relaxation as a Tool for Characterising the Adsorption Strength of Liquids inside Porous Materials. *Chem. - Eur. J.* **2014**, *20*, 13009−13015.
(38) Jameson, C. J. In *Gas Phase NMR*; Jacowski, K., Jaszunski, M., Eds.; The Royal Society of Chemistry: UK, 2016; Chapter 1, pp 1−51.
(39) Stallmach, F.; Pusch, A.-K. K.; Splith, T.; Horch, C.; Merker, S. NMR relaxation and diffusion studies of methane and carbon dioxide in nanoporous ZIF-8 and ZSM-58. *Microporous Mesoporous Mater.* **2015**, *205*, 36−39.
(40) Duncan, T.; Dybowski, C. Chemisorption and surfaces studied by nuclear magnetic resonance spectroscopy. *Surf. Sci. Rep.* **1981**, *1*, 157−250.
(41) Kärger, J.; Pfeifer, H. N.M. R self-diffusion studies in zeolite science and technology. *Zeolites* **1987**, *7*, 90.
(42) Kimmich, R. *NMR Tomography, Diffusometry, Relaxometry*; Springer: Berlin, Heidelberg, 1997; pp 1−474.
(43) Chmelik, C.; Kärger, J.; Wiebcke, M.; Caro, J.; van Baten, J.; Krishna, R. Adsorption and diffusion of alkanes in CuBTC crystals investigated using infra-red microscopy and molecular simulations. *Microporous Mesoporous Mater.* **2009**, *117*, 22−32.
(44) Price, W. S. Pulsed-field gradient nuclear magnetic resonance as a tool for studying translational diffusion: Part 1. Basic theory. *Concepts Magn. Reson.* **1997**, *9*, 299−336.
(45) Topgaard, D.; Pines, A. Self-diffusion measurements with chemical shift resolution in inhomogeneous magnetic fields. *J. Magn. Reson.* **2004**, *168*, 31−35.
(46) Kärger, J.; Ruthven, D.; Theodorou, D. Elementary Principles of Diffusion. *Diffus. Nanoporous Mater.* **2012**, 1 DOI: 10.1002/9783527651276.
(47) Chmelik, C.; Freude, D.; Bux, H.; Haase, J. Ethene/ethane mixture diffusion in the MOF sieve ZIF-8 studied by MAS PFG NMR diffusometry. *Microporous Mesoporous Mater.* **2012**, *147*, 135−141.
(48) Díaz, K.; Garrido, L.; López-González, M.; Del Castillo, L. F.; Riande, E. CO_2 transport in polysulfone membranes containing zeolitic imidazolate frameworks as determined by permeation and PFG NMR techniques. *Macromolecules* **2010**, *43*, 316−325.
(49) Kong, X.; Scott, E.; Ding, W.; Mason, J. A.; Long, J. R.; Reimer, J. A. CO_2 dynamics in a metal-organic framework with open metal sites. *J. Am. Chem. Soc.* **2012**, *134*, 14341−4.
(50) Kong, X.; Deng, H.; Yan, F.; Kim, J.; Swisher, J. A.; Smit, B.; Yaghi, O. M.; Reimer, J. A. Mapping of functional groups in metal-organic frameworks. *Science* **2013**, *341*, 882−5.
(51) Marti, R. M.; Howe, J. D.; Morelock, C. R.; Conradi, M. S.; Walton, K. S.; Sholl, D. S.; Hayes, S. E. CO_2 Dynamics in Pure and Mixed-Metal MOFs with Open Metal Sites. *J. Phys. Chem. C* **2017**, *121*, 25778−25787.
(52) Couck, S.; Denayer, J. F.; Baron, G. V.; Rémy, T.; Gascon, J.; Kapteijn, F. An amine-functionalized MIL-53 metal- organic framework with large separation power for CO_2 and CH_4. *J. Am. Chem. Soc.* **2009**, *131*, 6326−6327.
(53) Bourrelly, S.; Llewellyn, P. L.; Serre, C.; Millange, F.; Loiseau, T.; Férey, G. Different adsorption behaviors of methane and carbon dioxide in the isotypic nanoporous metal terephthalates MIL-53 and MIL-47. *J. Am. Chem. Soc.* **2005**, *127*, 13519−13521.
(54) Zhang, Y.; Lucier, B. E.; Huang, Y. Deducing CO_2 motion, adsorption locations and binding strengths in a flexible metal−organic framework without open metal sites. *Phys. Chem. Chem. Phys.* **2016**, *18*, 8327−8341.
(55) Lucier, B. E. G.; Chan, H.; Zhang, Y.; Huang, Y. Multiple Modes of Motion: Realizing the Dynamics of CO Adsorbed in M-MOF-74 (M = Mg, Zn) by Using Solid-State NMR Spectroscopy. *Eur. J. Inorg. Chem.* **2016**, *2016*, 2017−2024.
(56) Banerjee, D.; Zhang, Z.; Plonka, A. M.; Li, J.; Parise, J. B. A calcium coordination framework having permanent porosity and high CO_2/N_2 selectivity. *Cryst. Growth Des.* **2012**, *12*, 2162−2165.
(57) Chen, S.; Lucier, B. E. G.; Boyle, P. D.; Huang, Y. Understanding the Fascinating Origins of CO_2 Adsorption and Dynamics in MOFs. *Chem. Mater.* **2016**, *28*, 5829−5846.
(58) Lin, J.-D.; Wu, S.-T.; Li, Z.-H.; Du, S.-W. A series of novel Pb (II) or Pb (II)/M (II)(M= Ca and Sr) hybrid inorganic−organic frameworks based on polycarboxylic acids with diverse Pb−O−M (M= Pb, Ca and Sr) inorganic connectivities. *CrystEngComm* **2010**, *12*, 4252−4262.
(59) Chui, S. S.-Y.; Lo, S. M.-F.; Charmant, J. P. H.; Orpen, A. G.; Williams, I. D. A Chemically Functionalizable Nanoporous Material $[Cu_3(TMA)_2(H2O)_3]n$. *Science* **1999**, *283*, 1148−1150.
(60) Wu, H.; Simmons, J. M.; Srinivas, G.; Zhou, W.; Yildirim, T. Adsorption Sites and Binding Nature of CO_2 in Prototypical MetalOrganic Frameworks: A Combined Neutron Diffraction and First-Principles Study. *J. Phys. Chem. Lett.* **2010**, *1*, 1946−1951.
(61) Schlayer, S.; Pusch, A.-K.; Pielenz, F.; Beckert, S.; Peksa, M.; Horch, C.; Moschkowitz, L.; Einicke, W.-D.; Stallmach, F. X-nuclei NMR self-diffusion studies in mesoporous silica foam and microporous MOF CuBTC. *Materials* **2012**, *5*, 617−633.
(62) Gul-E-Noor, F.; Mendt, M. Adsorption of Small Molecules on $Cu_3(btc)_2$and $MCu_3-_xZn_x(btc)_2$etal Organic Frameworks (MOF) As studied by Solid-State NMR. *J. Phys. Chem. C* **2013**, *3*, 7703−7712.
(63) Gul-E-Noor, F.; Michel, D. Investigation of the spin-lattice relaxation of ^{13} CO and ^{13} CO_2 adsorbed in the metal-organic frameworks $Cu_3(btc)_2$ and $Cu_{3x}Zn_x(btc)_2$. *J. Phys. Chem. C* **2013**, *117*, 7703.

DOI: 10.1021/acs.chemrev.7b00695
Chem. Rev. 2018, 118, 10033−10048

(64) Xiang, S.; Wu, X.; Zhang, J.; Fu, R.; Hu, S.; Zhang, X. A 3D canted antiferromagnetic porous metal-organic framework with anatase topology through assembly of an analogue of polyoxometalate. *J. Am. Chem. Soc.* **2005**, *127*, 16352−16353.
(65) Xiang, S.; He, Y.; Zhang, Z.; Wu, H.; Zhou, W.; Krishna, R.; Chen, B. Microporous metal-organic framework with potential for carbon dioxide capture at ambient conditions. *Nat. Commun.* **2012**, *3*, 954.
(66) Masala, A.; Grifasi, F.; Atzori, C.; Vitillo, J. G.; Mino, L.; Bonino, F.; Chierotti, M. R.; Bordiga, S. CO_2 Adsorption Sites in UTSA-16: Multitechnique Approach. *J. Phys. Chem. C* **2016**, *120*, 12068−12074.
(67) Liu, H.; Guo, P.; Regueira, T.; Wang, Z.; Du, J.; Chen, G. Irreversible Change of the Pore Structure of ZIF-8 in Carbon Dioxide Capture with Water Coexistence. *J. Phys. Chem. C* **2016**, *120*, 13287−13294.
(68) Pusch, A.-K.; Splith, T.; Moschkowitz, L.; Karmakar, S.; Biniwale, R.; Sant, M.; Suffritti, G. B.; Demontis, P.; Cravillon, J.; Pantatosaki, E.; Stallmach, F. NMR studies of carbon dioxide and methane self-diffusion in ZIF-8 at elevated gas pressures. *Adsorption* **2012**, *18*, 359−366.
(69) Liu, D.; Wu, Y.; Xia, Q.; Li, Z.; Xi, H. Experimental and molecular simulation studies of CO_2 adsorption on zeolitic imidazolate frameworks:ZIF-8 and amine-modified ZIF-8. *Adsorption* **2013**, *19*, 25−37.
(70) Burtch, N. C.; Jasuja, H.; Dubbeldam, D.; Walton, K. S. Molecular-level Insight into Unusual Low Pressure CO_2 Affinity in Pillared Metal Organic Frameworks. *J. Am. Chem. Soc.* **2013**, *135*, 7172−7180.
(71) Peksa, M.; Burrekaew, S.; Schmid, R.; Lang, J.; Stallmach, F. Rotational and translational dynamics of CO_2 adsorbed in MOF $Zn_2(bdc)_2(dabco)$. *Microporous Mesoporous Mater.* **2015**, *2*, 75−81.
(72) Forse, A. C.; Gonzalez, M. I.; Siegelman, R. L.; Witherspoon, V. J.; Jawahery, S.; Mercado, R.; Milner, P. J.; Martell, J. D.; Smit, B.; Blumich, B.; Long, J. R.; Reimer, J. A. Unexpected Diffusion Anisotropy of Carbon Dioxide in the Metal−Organic Framework Zn_2(dobpdc). *J. Am. Chem. Soc.* **2018**, *140*, 1663−1673.
(73) Bon, V.; Pallmann, J.; Eisbein, E.; Hoffmann, H. C.; Senkovska, I.; Schwedler, I.; Schneemann, A.; Henke, S.; Wallacher, D.; Fischer, R. A.; Seifert, G.; Brunner, E.; Kaskel, S. Characteristics of flexibility in metal-organic framework solid solutions of composition $[Zn_2(BME-bdc)_x(DB-bdc)_{2-x}dabco]_n$: In situ powder X-ray diffraction, in situ NMR spectroscopy, and molecular dynamics simulations. *Microporous Mesoporous Mater.* **2015**, *216*, 64−74.
(74) Stallmach, F.; Pusch, A. K.; Splith, T.; Horch, C.; Merker, S. NMR relaxation and diffusion studies of methane and carbon dioxide in nanoporous ZIF-8 and ZSM-58. *Microporous Mesoporous Mater.* **2015**, *205*, 36−39.
(75) Armstrong, R. Longitudinal Nuclear Spin Relaxation Time Measurements in Molecular Gases. *Can. J. Phys.* **1976**, *53*, 71.
(76) Wu, H.; Simmons, J. M.; Srinivas, G.; Zhou, W.; Yildirim, T. Adsorption sites and binding nature of CO_2 in prototypical metal-organic frameworks: A combined neutron diffraction and first-principles study. *J. Phys. Chem. Lett.* **2010**, *1*, 1946−1951.
(77) Xu, T.; Haw, J. F. The development and applications of CAVERN methods for in situ NMR studies of reactions on solid acids. *Top. Catal.* **1997**, *4*, 109−118.
(78) Hu, J. Z.; Hu, M. Y.; Zhao, Z.; Xu, S.; Vjunov, A.; Shi, H.; Camaioni, D. M.; Peden, C. H.; Lercher, J. A. Sealed rotors for in situ high temperature high pressure MAS NMR. *Chem. Commun.* **2015**, *51*, 13458−13461.
(79) Woelk, K.; Bargon, J. High-pressure NMR probes for the in situ investigation of gas/liquid reactions. *Rev. Sci. Instrum.* **1992**, *63*, 3307−3310.
(80) Washburn, K. E. Relaxation mechanisms and shales. *Concepts Magn. Reson., Part A* **2014**, *43A*, 57−78.
(81) Böhlmann, W.; Pöppl, A.; Sabo, M.; Kaskel, S. Characterization of the metal-organic framework compound $Cu_3(benzene1,3,5-tricarboxylate)_2$by means of ^{129}Xe nuclear magnetic and electron paramagnetic resonance spectroscopy. *J. Phys. Chem. B* **2006**, *110*, 20177−81.
(82) Etesse, P.; Zega, J. A.; Kobayashi, R. High pressure nuclear magnetic resonance measurement of spin-lattice relaxation and self-diffusion in carbon dioxide. *J. Chem. Phys.* **1992**, *97*, 2022−2029.
(83) Kim, J.; Abouelnasr, M.; Lin, L.-C.; Smit, B. Large-Scale Screening of Zeolite Structures for CO_2 Membrane Separations. *J. Am. Chem. Soc.* **2013**, *135*, 7545−7552.
(84) Lin, L.-C.; Kim, J.; Kong, X.; Scott, E.; McDonald, T. M.; Long, J. R.; Reimer, J. A.; Smit, B. Understanding CO_2 dynamics in metal-organic frameworks with open metal sites. *Angew. Chem., Int. Ed.* **2013**, *52*, 4410−3.

DOI: 10.1021/acs.chemrev.7b00695
Chem. Rev. 2018, 118, 10033−10048